Sound & Vibration 2025, 59(2), 1941.
https://doi.org/10.59400/sv1941

Article

Identification of vehicle suspension shock absorber rattle noise based on wavelet packet feature fusion and GWO-LSTM

Jie Hou[1,2], Hongwei Yi[1,2], Xingyu Xiang[1,2], Xiangyu Ni[3], Ruxue Dai[4], Xiaorong Huang[1,2,*]

[1] Vehicle Measurement Control and Safety Key Laboratory of Sichuan Province, Xihua University, Chengdu 610039, China
[2] Sichuan Engineering Research Center of Intelligent Control and Simulation Test Technology for New Energy Vehicles, Xihua University, Chengdu 610039, China
[3] State Key Laboratory of Intelligent Manufacturing of Advanced Construction Machinery, Xuzhou Construction Machinery Group, Xuzhou 211162, China
[4] School of Mechanical Engineering, Southwest Jiaotong University, Chengdu 610031, China
*** Corresponding author:** Xiaorong Huang, 1220190017@xhu.edu.cn

CITATION

Hou J, Yi H, Xiang X, et al. Identification of vehicle suspension shock absorber rattle noise based on wavelet packet feature fusion and GWO-LSTM. Sound & Vibration. 2025; 59(2): 1941. https://doi.org/10.59400/sv1941

ARTICLE INFO

Received: 26 October 2024
Accepted: 22 November 2024
Available online: 14 March 2025

Abstract: With the advancement of pure electric vehicles, the issue of rattle noise in suspension shock absorbers has increasingly become a critical factor affecting vehicle comfort. This paper proposes a method for rattle noise recognition based on wavelet packet feature fusion and the grey wolf optimizer-long short-term memory (GWO-LSTM) model, aimed at improving the accuracy and efficiency of rattle noise detection. The vibration signals of the shock absorbers are decomposed by wavelet packet decomposition (WPD), followed by extraction of wavelet packet energy (WPE) and wavelet packet fuzzy entropy (WPFE) features and feature fusion. Subsequently, the GWO algorithm is employed to optimize the hyperparameters of the LSTM model, enhancing classification performance. The results demonstrate that, compared to traditional methods, the GWO-LSTM model significantly improves classification accuracy and training efficiency, achieving an accuracy rate of 97.85%, particularly excelling in the recognition of both slight and serious rattle noise. This study provides an efficient and reliable solution for the automated evaluation of shock absorbers' rattle noise.

Keywords: wavelet packet energy (WPE); wavelet packet fuzzy entropy (WPFE); grey wolf optimizer (GWO); long short-term memory (LSTM)

1. Introduction

In recent years, as the automotive manufacturing and component industries have continued to evolve, the shift towards pure electric vehicles (PEVs) has become more pronounced [1]. This transition has led to improvements in controlling major vibration and noise sources associated with traditional powertrains. However, rattle noise caused by suspension shock absorber has gradually emerged as a significant issue [2,3]. Although significant progress has been made in improving shock absorber' noise reduction through advanced research and application in engineering, differentiation among shock absorbers that exhibit slight rattle noise issues remains challenging. In both vehicle road tests and rig tests, the majority of noisy shock absorbers exhibit similar characteristics, typically classified as having slight rattle noise. While this noise is relatively weak, it can still be perceived by sensitive passengers and easily detected by noise evaluation experts [4]. The absence of a clear evaluation standard for distinguishing slight noisy shock absorbers not only results in repetitive work and resource waste during shock absorber noise-reduction design but also hinders

technological advancement and industry growth. Therefore, it is essential to establish a reliable method for accurately identifying shock absorbers' rattle noise to support technological progress and meet the demands of the automotive industry.

Currently, evaluation methods of shock absorber rattle noise are primarily categorized into subjective vehicle-level evaluations and objective rig tests [5]. In vehicle-level evaluations, noise detection is often based on subjective assessments during vehicle road tests, relying on the human ear to perceive noise, and providing a direct reflection of driver experience [6,7]. Research show that shock absorber rattle noise is closely related to the vibration characteristics of its mounting position [8,9]. Traditional road tests, however, require evaluations across various road conditions and speeds, which significantly increases the time, labor, and cost associated with testing [10]. In contrast, rig tests offer a more efficient solution for shock absorber noise evaluation by eliminating the complexities of full vehicle testing. Studies comparing the root-mean-square (RMS) vibration acceleration at the shock absorber piston rod's top during road and rig tests have shown a strong correlation with noise levels, confirming that vibration characteristics at the piston rod tip correspond to noise severity [11]. This indicates that simpler rig tests can partially replace more complex vehicle road tests for noise evaluation. Additional research [12] has validated the similarity between vibration acceleration signals in both rig and road tests, particularly within specific frequency ranges, further supporting the consistency of both methods. While rig tests are more efficient and cost-effective than vehicle-level tests, determining appropriate excitation frequencies, amplitudes, and piston rod velocities remains critical. Typically, multiple test conditions must be evaluated to identify the most noise-inducing scenarios that correlate with subjective assessments, which adds complexity to data processing. To improve shock absorber noise evaluation efficiency and reduce costs, this study establishes a standardized framework for both subjective and objective analyses. The proposed approach specifies rig test conditions and criteria for noise evaluation, aiming to provide practical guidance for engineering applications.

Presently, noise recognition and analysis methods for shock absorber primarily involve simulation-based and data-driven approaches. Simulation models, grounded in physical principles, offer strong interpretability but face limitations in handling complex conditions and require high computational costs [13]. Data-driven methods, by contrast, leverage extensive experimental data to automatically extract noise features, offering higher modeling efficiency and adaptability, though they rely heavily on high-quality data [14]. Among data-driven models, Long Short-Term Memory (LSTM) networks and Convolutional Neural Networks (CNN) are widely used. LSTM is particularly effective for processing time-series data, capturing temporal features of noise signals [15], while CNNs excel in extracting local spatial features, particularly when analyzing the frequency characteristics of vibration signals [16]. Although these models effectively recognize shock absorber noise, their complexity and the need for parameter tuning increase training time. To address these challenges, the Grey Wolf Optimizer (GWO), a powerful optimization tool that mimics the hunting behavior of wolves, has shown superior performance in global search capabilities, convergence speed, and stability compared to traditional algorithms like genetic algorithms [17,18]. Studies have demonstrated that integrating

GWO with LSTM models can effectively optimize model parameters, improving the accuracy and robustness of shock absorber noise detection [19]. Therefore, this paper incorporates GWO to optimize LSTM model parameters, aiming to further enhance the efficiency and accuracy of shock absorber rattle noise recognition.

In data-driven models, the quality of input features directly impacts recognition performance.

At present, the methods of feature extraction are used in the identification of rattle noise of vehicle shock absorber, the analysis of interior noise and the fault diagnosis of engine in the field of automobile. In the aspect of feature extraction methods for shock absorber vibration data, the methods are mainly classified into time-domain and frequency-domain features. Time-domain features, such as peak-to-peak values, root-mean-square values, and energy values [20], offer a straightforward reflection of signal intensity and variability, making them easy to compute and interpret. However, they often fail to reveal the frequency components of the signal, limiting their ability to capture the detailed frequency information of shock absorber noise [21]. Frequency-domain features, derived through spectral analysis, can effectively extract frequency characteristics of vibration signals, offering a more detailed representation of noise structure, though they require more computational resources [22,23]. In the field of in-vehicle noise analysis, combining time-domain and frequency-domain features for noise recognition has been shown to yield excellent results [24,25]. In the analysis of engine fault diagnosis, the feature extraction methods such as fractal correlation dimension, wavelet energy, and entropy, are employed to encapsulate the distinctive attributes of engine fault signals. These methods enhance the precision of diesel engine fault diagnosis, facilitating a more robust and reliable analytical process [26].

This approach leverages the strengths of both feature types, enhancing the model's ability to handle complex signals. In this study, based on the mechanisms behind shock absorber rattle noise, wavelet packet transform (WPD) is used for feature extraction, allowing for multi-scale, multi-frequency analysis [27]. Further feature fusion integrates the extracted features into the recognition model's input, improving the accuracy and robustness of shock absorber noise detection.

Based on the above analysis, this paper presents the following contributions: 1) A wavelet packet energy (WPE) and wavelet packet fuzzy entropy (WPFE)-based feature extraction method is proposed for analyzing noise characteristics of automotive suspension shock absorbers. This method identifies key features associated with structure-borne noise inside the vehicle and generates fused features. 2) A GWO-LSTM method is introduced to address the uncertainty in LSTM model parameter tuning. GWO is employed to intelligently optimize learning rate and the number of cells in the hidden layer of LSTM parameters, yielding an optimal parameter set in a shorter time, enhancing the model's prediction accuracy.

The paper is structured as follows: Section 2 introduces the WPD feature extraction method and the GWO-LSTM model. Section 3 outlines the procedures for vehicle tests and rig tests for shock absorber rattle noise evaluation, analyzing both subjective and objective test results. WPD is then applied to extract energy, fuzzy entropy, and fused features from the objective data. Section 4 presents the GWO-LSTM-based shock absorber rattle noise recognition model, comparing its predictive

performance with other models. Section 5 concludes the study. The architecture of this study is visually represented in **Figure 1**.

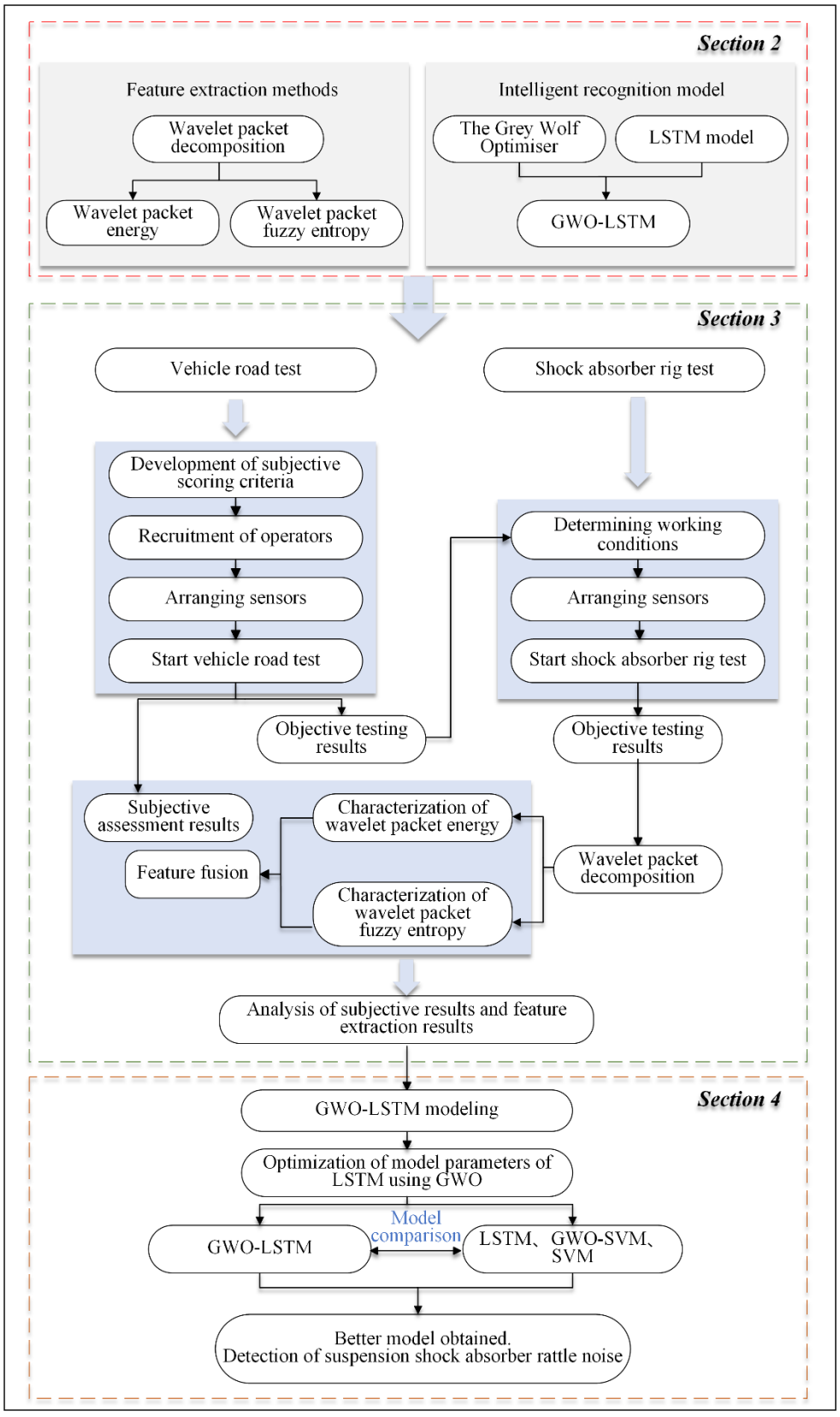

Figure 1. Research scheme of identification of shock absorber rattle noise.

2. Research method

2.1. Brief introduction of WPD

WPD is an advanced signal processing method developed on wavelet transform, which effectively extracts the time-frequency characteristics of a signal by decomposing the signal in multiple scales and resolutions [28]. Unlike the traditional wavelet transform, which decomposes only the low-frequency components, WPD decomposes both the low-frequency and high-frequency components of the signal, enabling a finer analysis over the full frequency range. Therefore, WPD has significant advantages in dealing with non-stationary signals [29].

In the process of WPD, the signal $x(t)$ is decomposed into multiple layers, each containing a number of nodes, each representing the signal in a specific frequency range. The signal $x(t)$ is decomposed by WPD in j layers and the subset signal obtained is $W_{j,n}(t)$, where n is the node number of the layer. Each node signal $W_{j,n}(t)$ can be further decomposed into two sub-node signals by recursive decomposition of low-pass and high-pass filters. The sub-node signals $W_{j+1,2n}(t)$ and $W_{j+1,2n+1}(t)$ of the n nodes of j layers are calculated as follows:

$$W_{j+1,2n}(t) = \sum_k h(k) W_{j,n}\left(t - 2^j k\right); W_{j+1,2n}(t) = \sum_k h(k) W_{j,n}\left(t - 2^j k\right) \quad (1)$$

where, $W_{j+1,2n}(t)$ indicates a lower frequency signal generated by the current node, $h(k)$ is the low-pass filter. 2^j adjusts signal resolution, $W_{j+1,2n+1}(t)$ indicates a higher frequency signal generated by the current node, $g(k)$ is the high-pass filter.

Through the above recursive decomposition process, the signal is refined layer by layer until the number of layers is reached. The three-layer WPD is shown in **Figure 2**, U3 represents the original signal, and U21 and U22 represent the high-frequency and low-frequency portions, respectively [30].

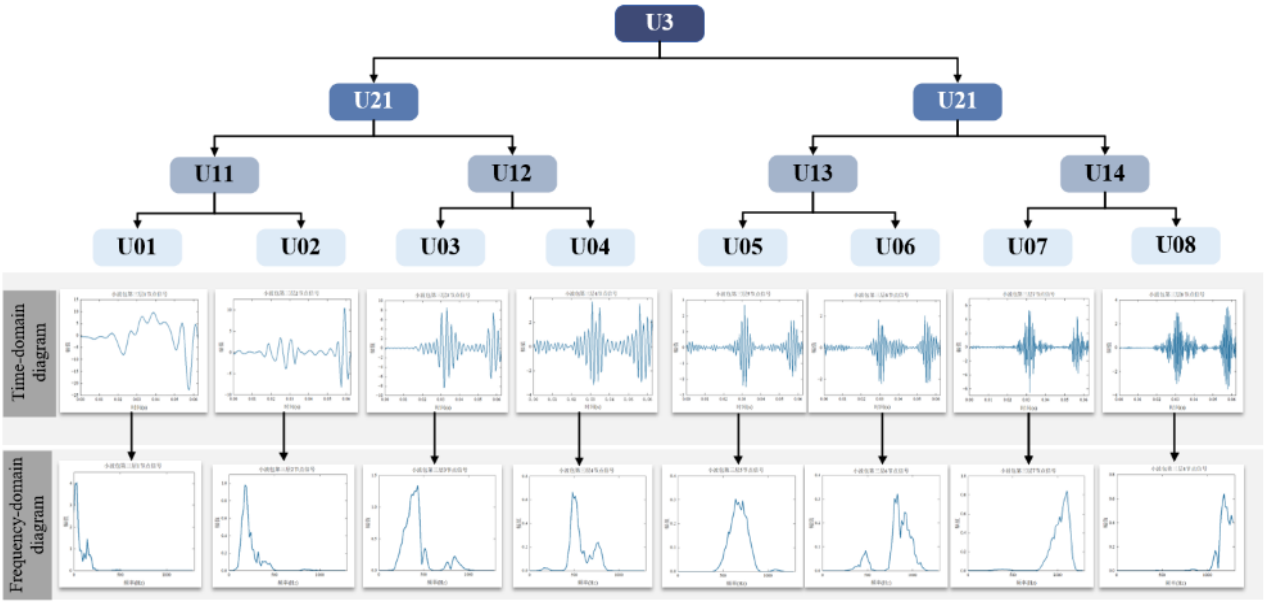

Figure 2. the three-layer WPD.

2.1.1. The method of WPE for feature extraction

WPE is an effective method for signal feature extraction. WPE reflects the energy distribution of the signal in each frequency band by summing the squares of the decomposition coefficients in each band, thus quantifying the local characteristics of the signal [31]. Due to its good time-frequency resolution, WPE shows excellent performance in processing non-stationary signals, especially in vibration signals and engineering data analysis under noise interference [32].

The original signal $\{x(n)|n = 1,2, \dots, N\}$ is decomposed and reconstructed through j layers of WPD, and the whole frequency band is decomposed to correspond to 2^j sub-bands, defining the energy E_{n_w} of the wth sub-band as:

$$E_{n_w} = \sum |P_w|^2, w = 0,1, \cdots 2^j - 1 \tag{2}$$

where, P_w is the wth wavelet packet coefficient under this decomposition level. Then the original signal $x(t)$ is characterized by the band energy after the decomposition, as shown:

$$E_{n_j} = \left| E_{n_0}, E_{n_1}, E_{n_2} \cdots E_{n_{2^{j-1}}} \right| \tag{3}$$

2.1.2. The method of WPFE for feature extraction

Fuzzy entropy (FE) is a method to quantify the complexity of time series. The complexity is evaluated by calculating the similarity between different states in the time series. The FE is more effective in extracting signal features and identifying complex dynamic changes when dealing with noisy and non-stationary signals such as engineering data and vibration signals [33]. When analyzing the vibration signal of the shock absorber, the WPFE can represent the complexity and uncertainty of the signal.

The original signal is decomposed and reconstructed through j layers of WPD, wavelet packet coefficients series $\{f(n)|n = 1,2, \dots, N\}$, The calculation steps of WPFE are as shown [34]:

$$FuzzyEn(N, m, r) = ln\frac{\Psi^m(r)}{\Psi^{m+1}(r)}; \Psi^m(r) = \frac{1}{N-m+1}\sum_{i=1}^{N-m+1}\left\{\frac{1}{N-m}\sum_{j=1, j\neq i}^{N-m+1} D_{ij}^m\right\} \tag{4}$$

where, m is the embedding dimension, r is tolerance, N is the number of data, D_{ij}^m is distance related items.

2.2. The proposed of GWO-LSTM

2.2.1. Brief introduction of long short-term memory

LSTM is a special type of Recurrent Neural Network (RNN) for processing and modeling long-term dependency problems in long sequence data [35]. By introducing memory units and gating mechanisms (including input gates, forgetting gates, and output gates), LSTM is able to efficiently capture and maintain long-term information during training, while suppressing problems such as gradient vanishing and gradient explosion. Due to its excellent ability to process temporal data, LSTM is widely used in the fields of time series prediction, natural language processing, and speech

recognition [36]. The structure of LSTM network is shown in **Figure 3a**, where the internal structure of cells is shown in **Figure 3b**.

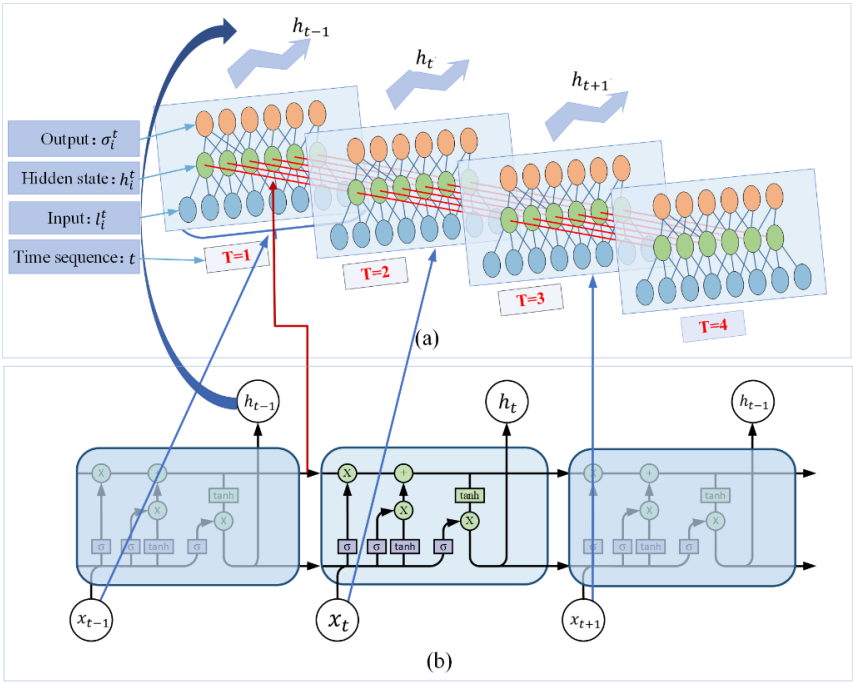

Figure 3. The structure of LSTM network and internal structure of cell. **(a)** The structure of LSTM network; **(b)** The internal structure of cell.

The core of LSTM is the memory unit, which realizes precise control of information through a "gate mechanism", allowing the network to selectively remember, update or forget certain information. Specifically, LSTM is able to dynamically adjust the cell state through the following steps [37,38]:

The forgetting gates determine the portion of the previous cell state C_{t-1} to be retained by a sigmoid activation function. The sigmoid function outputs a value between 0 and 1, which is multiplied by the previous cell state, and "0" for all oblivion and "1" for all retention. The operation of the forgetting gate is given by the following equation:

$$f_t = \sigma\left(W_f.[h_{t-1}, x_t] + b_f\right) \tag{5}$$

where f_t is the output of the forgetting gate, W_f and b_f are the weight matrix and bias vector, respectively, h_{t-1} is the hidden state at the previous moment, x_t is the current input, and σ denotes the sigmoid function.

The input gate determines what new information will be added to the cell state. First, a sigmoid function is used to determine how much information should be introduced from the current input x_t, followed by a $\tan h$ layer to generate new candidate cell states. The mathematical description of these steps is as follows:

$$i_t = \sigma(W_i.[h_{t-1}, x_t] + b_i) \tag{6}$$

$$c_t = \tan h\,(W_c.[h_{t-1}, x_t] + b_c) \tag{7}$$

where i_t is the output of the input gate, c_t is the candidate cell state, W_i, W_c and b_i, b_c are the weight matrix and bias vector, respectively.

By combining the output of the forgetting gate f_t and the output of the input gate i_t, the LSTM updates the current cell state C_t. This process is represented by the following equation:

$$C_t = f_t \times C_{t-1} + i_t \times c_t \tag{8}$$

where C_t is the updated cell state that contains the previous moment information and the new information at the current moment.

The output gate controls the output part of the LSTM. First, the sigmoid function determines which information in the cell state C_t needs to be output, and then the cell state is adjusted by the $\tan h$ function and multiplied with the result of the output gate to obtain the hidden state h_t at the current moment.

$$o_t = \sigma(W_o.[h_{t-1}, x_t] + b_o) \tag{9}$$

$$h_t = o_t \times \tan h\ (C_t) \tag{10}$$

Through the gating mechanism, LSTM is able to effectively handle the information flow in long sequence data, which significantly enhances the ability to model long time dependencies.

2.2.2. GWO-LSTM modeling

LSTM can effectively deal with long and short-term dependence problems in time series. However, the performance of LSTM models is highly dependent on the settings of hyperparameters, including the number of hidden layers, the number of cells per layer, the learning rate and the batch size [39]. If these parameters are not properly configured, the training process of the model will become very time-consuming and may lead to a decrease in the model accuracy. Traditional hyper-parameter optimization methods, such as grid search and stochastic search, are usually inefficient and difficult to find the global optimal solution. Therefore, introducing effective optimization algorithms becomes the key to improve the performance of LSTM models.

GWO is a group intelligent optimization algorithm simulating the hunting behavior of grey wolves, which has the advantages of fast convergence, simple parameter setting, easy implementation, and outstanding performance in global optimization search [40]. GWO achieves global exploration of the search space and localization by simulating the leadership hierarchical structure of a grey wolf group and the prey rounding strategy, and by utilizing synergistic roles of four roles, namely α, β, δ, and ω, to achieve global exploration and local exploitation. Specifically, the individuals of the grey wolf group are divided into four hierarchical roles: α-wolf (leader), β-wolf (second leader), δ-wolf (third leader), and ω-wolf (ordinary member). Among them, α-wolf represents the optimal position of the current solution, β-wolf and δ-wolf represent the second and third best solutions, respectively, while ω-wolf is the other ordinary pack members. This hierarchical structure allows the GWO to synthesize information from different individuals to guide the search direction during the search process. α, β and δ wolves' positions are considered to be

the best estimates of the hunting target, and the other ω wolves update their own positions based on the positions of these three, thus approaching the optimal solution [41]. The position update of the gray wolf is as following:

$$\vec{X}(t) = \vec{X}_p(t) \cdot \vec{A} \times \vec{D} \tag{11}$$

$$\vec{D} = \left|\vec{C} \times \vec{X}_p(t) - \vec{X}(t)\right| \tag{12}$$

where t denotes the current number of iterations, $\vec{A}$ and $\vec{C}$ denote the coefficient vectors controlling convergence and exploration, $\vec{X}_p$ denotes the position vector of the prey, and $\vec{X}$ denotes the current position vector of the individual gray wolf.

The parameter vectors $\vec{A}$ and $\vec{C}$ are determined by the following equations, respectively:

$$\vec{A} = 2\vec{a} \times \vec{r}_1 - \vec{a};\ \vec{C} = 2\vec{r}_2;\ \vec{a} = 2 \cdot 2\frac{t}{T} \tag{13}$$

where the vector $\vec{a}$ is a control parameter that decreases linearly with the number of iterations, $\vec{r}_1$ and $\vec{r}_2$ are random vectors uniformly distributed between 0 and 1, and T is the maximum number of iterations. The adaptive tuning factor and information feedback mechanism of the GWO can dynamically adjust the searching direction and step size during the optimization process, thus improving the efficiency and accuracy of the search.

When applying GWO to the optimization of LSTM models, the fitness function of GWO can be defined as the prediction error of the LSTM model on the validation set, which is usually measured by the mean squared error (MSE) or root mean square error (RMSE):

$$\text{MSE} = \frac{1}{n}\sum_{i=1}^{n}(y_i - \hat{y}_i)^2 \tag{14}$$

where y_i is the actual value and $\hat{y}_i$ is the predicted value of the LSTM model. The optimization process includes the following steps:

First, initialize the position of the grey wolf population, randomly set the hyperparameters of the LSTM model; Second, search for the optimal hyperparameter combinations by iteratively updating the position of the grey wolves; Finally, select the optimal hyperparameter combination based on the values of the fitness function, and apply them to the LSTM model. The global searching ability of the GWO enables it to effectively avoid falling into the local optimum, which improves the LSTM model's generalization ability and prediction accuracy. The computational logic of the proposed LSTM model based on the GWO algorithm is shown in **Figure 4** [42].

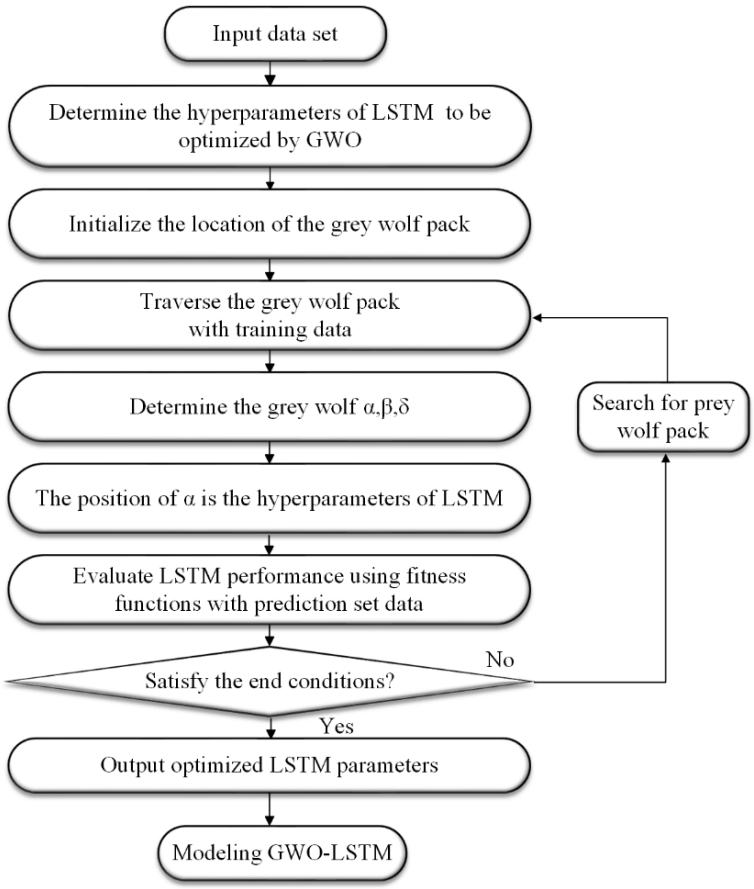

Figure 4. The logic of GWO-LSTM model.

Introducing GWO to optimize the hyperparameters of LSTM model can not only significantly reduce the model training time, but also improve the prediction performance of the model, making it more suitable for complex time series analysis tasks. Through this combination, the advantages of LSTM in dealing with long sequence dependency problems can be fully exploited, while the optimization capability of GWO is used to achieve a global improvement of the model performance.

3. Vehicle suspension shock absorber rattle noise experiment

To identify the rattle noise in the shock absorbers of new energy vehicles, it is necessary to quantify the rattle noise. Using a certain vehicle model, this section designs both vehicle road tests and rig tests to address the characteristics of shock absorber rattle noise.

3.1. Shock absorber rattle noise road test and subjective evaluation

Quantifying shock absorber rattle noise requires subjective evaluation, so a full-vehicle road test is conducted first. Rattle noise in shock absorbers typically occurs when vehicles travel at low speeds on uneven roads. After conducting extensive road tests, the vehicle speed was controlled at approximately 30 km/h on ripple road. The test was equipped with four no rattle shock absorbers, and for each test, either the front or rear two shock absorbers were replaced with test samples, while the other two remained no rattle. A total of 50 shock absorbers with varying degrees of rattle noise

were tested. To capture the road-induced excitation, vibration acceleration sensors were installed near the steering knuckle of the lower control arms on both sides of the front suspension. This allowed analysis of the vibration acceleration signals at the steering knuckle to determine the excitation conditions for the bench test. To ensure the accuracy of the test, no large sound sources or reflective objects were present within 20 m of the test site, and all vehicle doors and windows were closed. Vibration signals were collected using the LMS Test. Lab system, with a sampling frequency of 2560 Hz, a frequency resolution of 1 Hz, and a sampling time of 10 s.

For subjective evaluation, professional evaluators were recruited to assess the shock absorber rattle noise during the vehicle road test. Given that rattle noise is relatively simple in nature, a three-level subjective rating scale was used. As shown in **Figure 5c**, a score of 1 represents serious rattle noise, 2 represents slight rattle noise, and 3 indicates no rattle noise [43]. Twenty evaluators participated in the test, and the average subjective score for rattle noise was used for subsequent modeling and analysis. **Figure 5** illustrates the process of the vehicle road test and subjective evaluation of shock absorber rattle noise, where each rattle noise score is derived from the mean score of the evaluators.

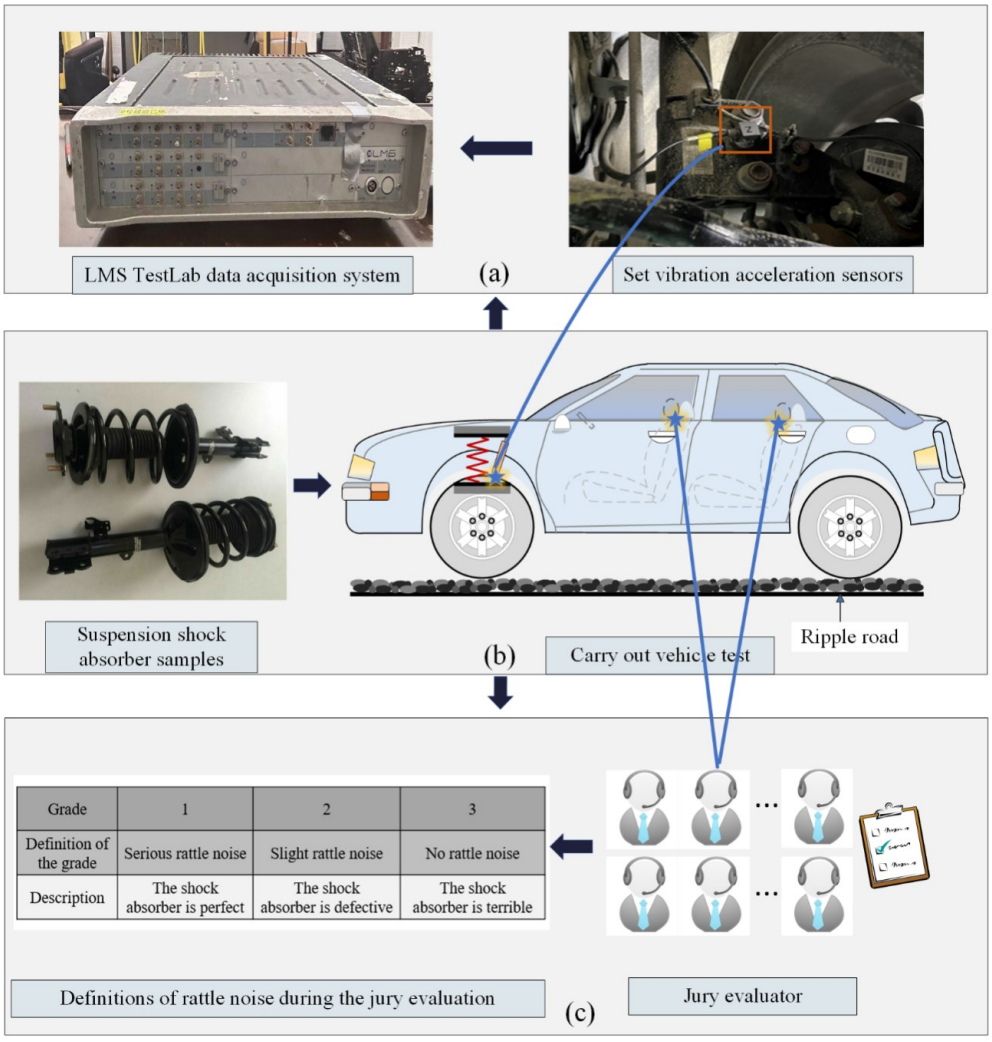

Figure 5. the process of the vehicle road test and subjective evaluation. **(a)** Data acquisition system and setting sensors; **(b)** The vehicle road test of shock absorber rattle noise; **(c)** Subjective evaluation.

3.2. Shock absorber rattle noise rig test and objective evaluation

While vehicle testing offers high accuracy, it is inefficient, costly, and lacks consistency in results. To address these limitations, rig testing is introduced as a cost-effective and efficient alternative to identify rattle noise through vibration analysis, referred to as "substituting vibration for sound". This method is based on the results of vehicle tests and follows the approach outlined in reference [3]. The primary factor influencing shock absorber rattle noise is the excitation frequency. As shown in **Figure 6**, the vibration signals from the suspension lower arm indicate that the primary road excitation frequency is approximately 16 Hz. Therefore, in the rig test, the vertical excitation condition is set to a sinusoidal signal with a frequency of 16 Hz, and the excitation velocity is chosen as 0.12 m/s, which corresponds to the valve opening velocity of the shock absorber piston at low speed. During the test, the shock absorber fixture and the installation of vibration sensors are illustrated in **Figure 7**, and the sampling frequency is maintained consistent with that of the road test. The rig test used is the MTS 850 Shock Absorber Comprehensive Performance Testing Machine, manufactured by MTS Corporation, USA, with the test environment controlled at 20 ℃ ± 5 ℃.

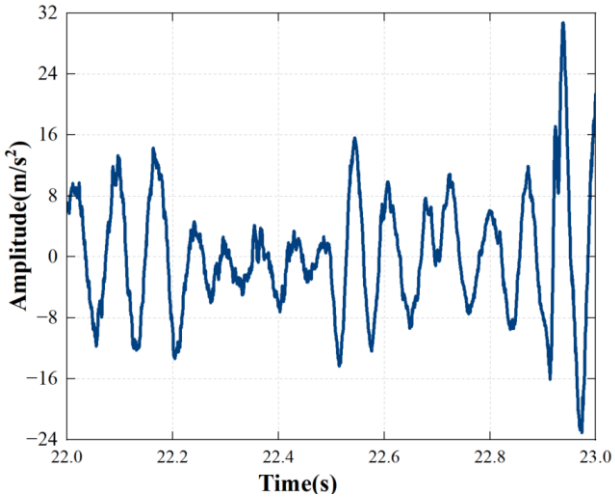

Figure 6. the vibration signals from lower suspension arm.

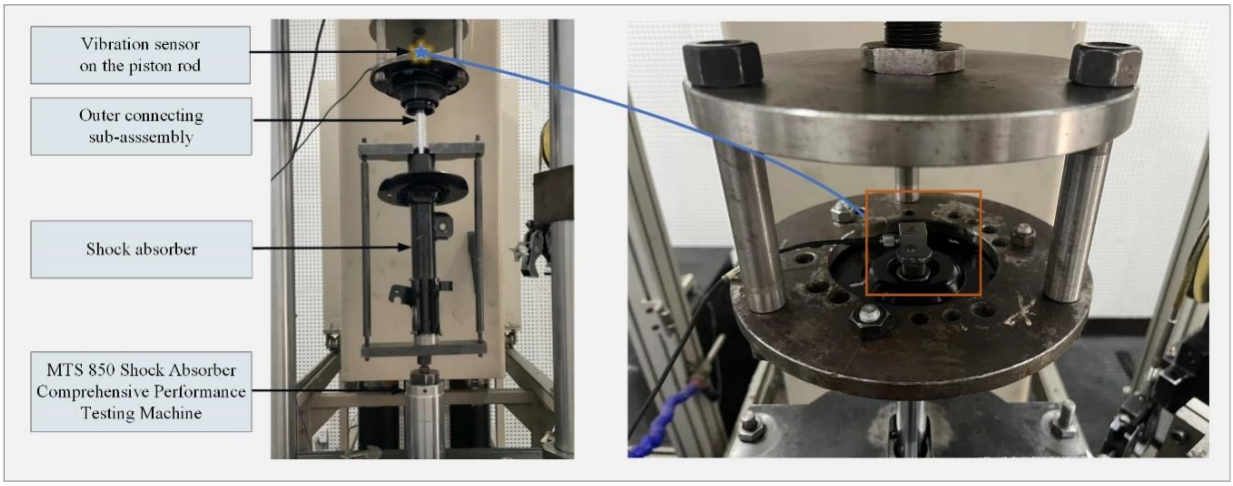

Figure 7. The shock absorber fixture and the installation of vibration sensors.

The time-domain and frequency-domain comparisons of the vibration signals of the shock absorber samples exhibiting three levels of rattle noise during the rig test are shown in **Figure 8**. As shown in **Figure 8a**, it is difficult to differentiate between the various rattle noise by observing the time-domain signals alone, as they contain a significant amount of redundant information, making it challenging to accurately and efficiently identify shock absorber rattle noise. However, the frequency-domain analysis in **Figure 8b** reveals that, although the amplitude of the vibration acceleration signals in the 200 Hz to 600 Hz range partially reflects the noise level, this simple metric is insufficient for accurately identifying a large number of shock absorber rattle noise. Therefore, more advanced signal processing methods and effective feature extraction techniques are required to distinguish between different levels of rattle noise.

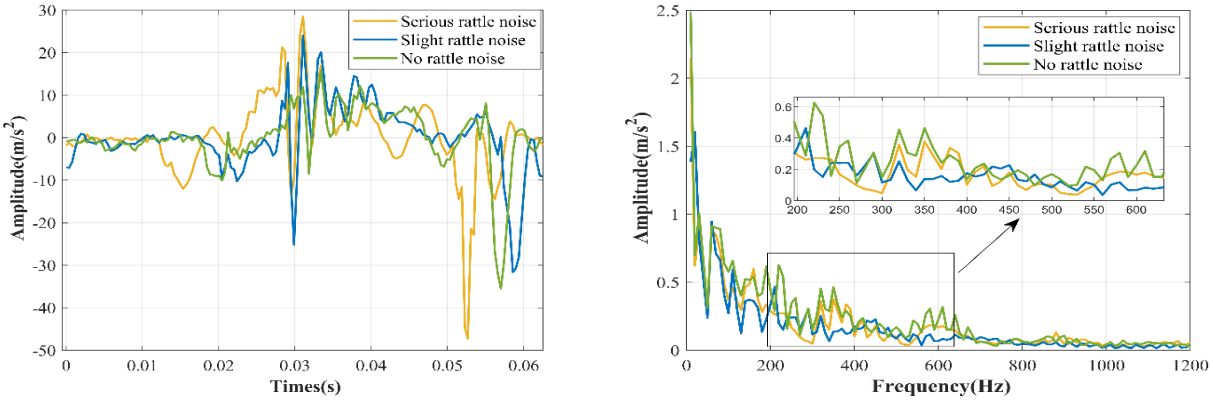

Figure 8. The comparison of three levels of rattle noise in time-domain and frequency-domain. **(a)** Time-domain; **(b)** Frequency-domain.

3.3. Feature extraction based on WPD

3.3.1. WPE feature extraction

When processing the vibration signals at the piston rod end using WPD, selecting an appropriate basis function of WPD and the number of decomposition levels is a critical step. Through multiple experimental comparisons, it was found that the collected signals show a strong correlation with Daubechies wavelets when shock absorber rattle noise occurs. Thus, the Daubechies wavelet (db10) known for its continuity and compact support was selected as basis function. The optimal number of decomposition levels was determined based on the signal's sampling frequency and the characteristic frequency of the rattle noise. So, with a sampling frequency of 2560 Hz and rattle noise concentrated in the 200–600 Hz range, a three-level WPD can divide the signal into eight sub-bands, which sufficiently meets the analysis requirements.

The energy of each node was calculated using Equation (2), and the results are shown in **Figure 9**. The comparison reveals that WPE correlates positively with the severity of rattle noise, particularly within the characteristic frequency bands, aligning with the test results.

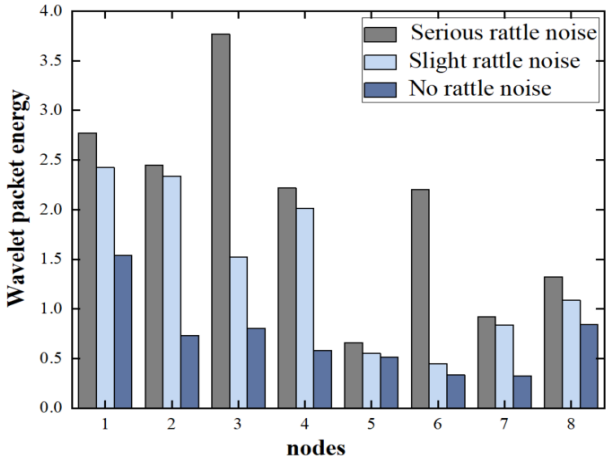

Figure 9. The distribution of WPE.

3.3.2. WPFE feature extraction

Based on the rig test data, when shock absorber rattle noise occurs, the vibration signals at the piston rod end generate specific frequency components. These components are first decomposed using WPD and then further processed through FE for feature extraction. The calculation of FE involves several parameters, including embedding dimension (m), similarity tolerance (r), and gradient (n). The embedding m determines the amount of information during sequence reconstruction, while the similarity r is usually selected as $(0.15\sim0.25)\times td$, where Std represents the standard deviation of the signal sequence, ensuring the statistical stability of the similarity calculation. The n reflects the contribution of vectors to the similarity computation, with larger values of n giving more weight to closer vectors. However, excessively large values of n can result in the loss of detail. After multiple rounds of data processing and parameter optimization, the final FE parameters were set as: embedding dimension $m=2$, gradient $n=2$, and similarity tolerance $r=(0.15-0.25)\times Std$.

To ensure good separability of features corresponding to different rattle noise levels, WPD coefficients of the vibration signals at the piston rod end were used. The FE coefficients for the eight decomposed wavelet packet coefficients were calculated using Equation (4), and the results are presented in **Figure 10**. The comparison indicates that in the characteristic frequency bands associated with rattle noise, the FE coefficients of shock absorbers without rattle noise are significantly higher than those with slight or serious rattle noise. This is because shock absorbers with no rattle noise exhibit more regular vibration characteristics, leading to higher fuzzy entropy values, whereas the presence of rattle noise introduces uncertainties in the shock absorber's reciprocating motion, resulting in lower FE values. Thus, WPFE effectively extracts rattle noise features from the perspective of signal uncertainty, contributing to more accurate shock absorber rattle noise evaluation.

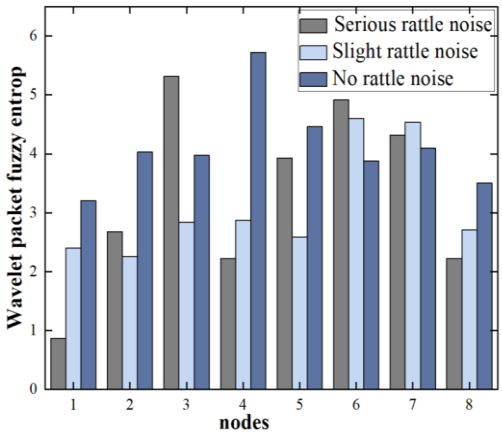

Figure 10. The distribution of WPFE.

3.3.3. Wavelet packet feature fusion

WPE and WPFE extract shock absorber rattle noise features from the perspectives of energy intensity and signal uncertainty, respectively. Since both features are derived from WPD, they exhibit consistency in feature dimensions, facilitating feature fusion. In this study, WPE and WPFE are fused to retain more comprehensive feature information related to shock absorber rattle noise. However, due to differences in dimension and magnitude between the two features, they need to be normalized before fusion.

The fusion feature of WPE and WPFE can be implemented in MATLAB. The feature matrices of WPE and WPFE are cross-merged, resulting in each sample containing two feature dimensions, WPE and WPFE. The specific implementation process is illustrated in **Figure 11**.

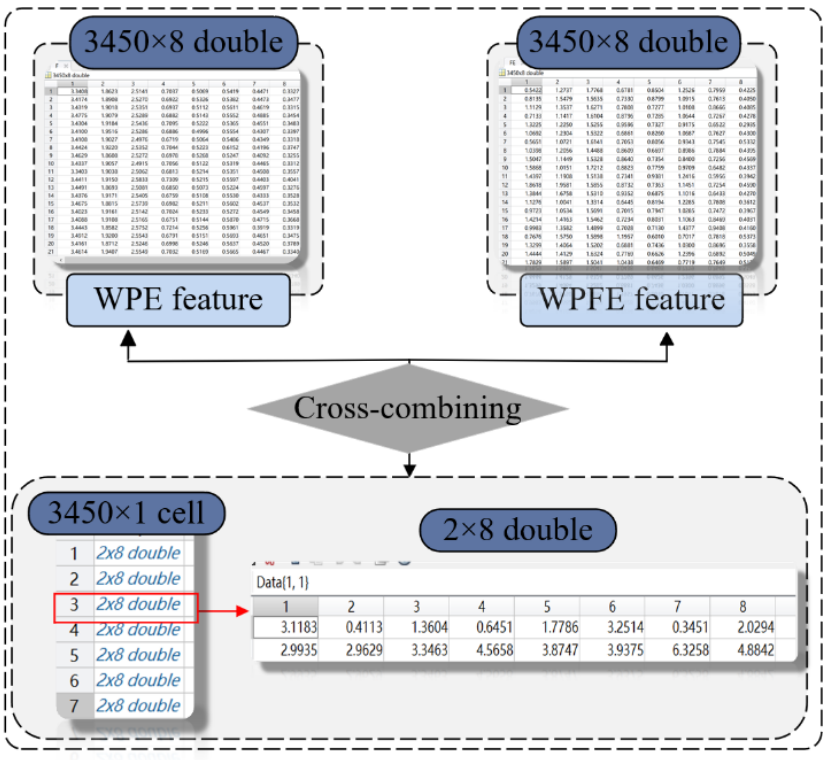

Figure 11. The specific implementation process of fusion feature.

4. Prediction and verification of shock absorber rattle noise

After the feature extraction in the previous section, the GWO-LSTM model is introduced to identify shock absorber rattle noise. Then its identification performance is compared with LSTM, SVM, GWO-SVM and GWO-CNN models. All the computational experiments were implemented in MATLAB 2023a. To account for the stochastic nature of intelligent algorithms, a total of 20 computational experiments were conducted. The average performance is reported in the following study.

4.1. Development of GWO-LSTM model

Eight frequency-band features obtained through wavelet packet feature fusion were selected as the input to the model, with different shock absorber rattle noise as the output (label 1 for serious rattle noise, label 2 for slight rattle noise, and label 3 for no rattle noise). During the model construction, two hyperparameters of the LSTM model, learning rate and the number of units in hidden layer, were optimized using the GWO algorithm. First, the upper and lower bounds of the learning rate and the number of cells in hidden layer were set, ranging from 0.001 to 0.01 and 10 to 30, respectively. Then, the parameter combinations were randomly initialized and assigned to the model for training. The error between the predicted and the true of classification value was used as the fitness function, and the GWO algorithm iteratively updated the parameter combinations. In the end, optimal parameters for the LSTM model were obtained. The parameter optimization process of the LSTM model is shown in **Figure 12**, and its computational logic referred to the logic of GWO-LSTM, as shown in **Figure 4**. The parameters of LSTM and GWO algorithm are presented in **Table 1**.

Table 1. GWO-LSTM parameters setting.

Algorithm type	Parameters type	value
LSTM	Input dimension	2
	Number of input features	8
	Maximum number of iterations	50
	Number of the hidden layers	4
	Forgetting rate	0.2
	Number of categories	3
	Optimization range of the number of cells	[10,30]
	Optimization range of Learning rate	[0.001,0.01]
GWO	Maximum number of iterations	15
	Number of optimized variables	2
	Population size	5

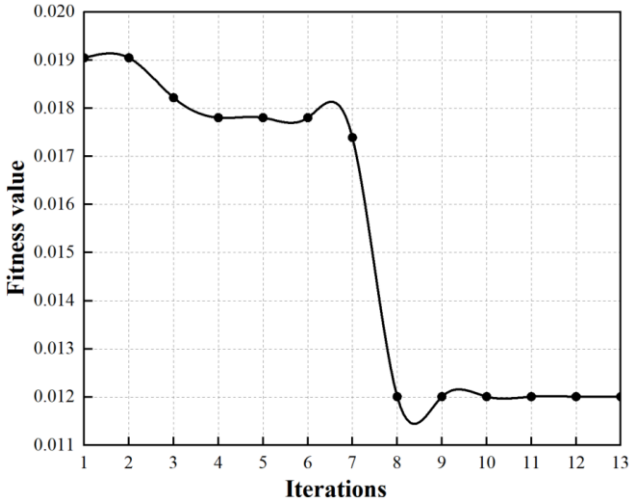

Figure 12. GWO-LSTM fitness curve.

As shown in **Figure 12**, during the optimization of different parameter combinations for the LSTM model, the convergence curve was generated. It is evident that the fitness value showed a continuous downward trend, as the number of iterations increased. After the 8th iteration, the convergence curve gradually became smoother, and after the 9th iteration, the fitness value essentially reached a stable state. Ultimately, the lowest root mean square error (RMSE) was 0.012, corresponding to the optimal parameter combination of a learning rate of 0.009 and 17units in the hidden layer. This indicates that the optimization performed by the GWO algorithm effectively improved the model's convergence efficiency and ensured a low prediction error.

4.2. Prediction results and analysis

Based on the GWO-LSTM model constructed in this study, experiments were conducted to identify rattle noise in shock absorbers by using WPE feature, WPFE feature and the fused feature as inputs. 3450 samples were divided into a training set and a test set according to 7:3. **Table 2** compares the classification accuracy and running time of shock absorber rattle noise using different features as inputs to the GWO-LSTM model. Among the single-feature recognition results, the classification accuracy of WPE was relatively high, reaching 93.66%. However, the runtime showed a longer convergence time of the model, at 70 s, indicating lower training efficiency. In contrast, the classification accuracy of WPFE was only 64.00%, but its convergence time was relatively shorter, at 37 s, showing higher training efficiency. The reason for this difference lies in the nature of the features: WPE represents the energy of specific frequency bands and has clear physical significance, especially in the low and mid-frequency ranges, which aligns with the spectral characteristics of the shock absorber piston rod signal. On the other hand, WPFE is mainly used to analyze the complexity of the signal, lacking clear physical meaning, leading to its lower classification accuracy.

Table 2. Comparison of recognition effects of GWO-LSTM model with different feature subsets.

Feature subset type	Recognition accuracy	Recognition efficiency
WPE feature	93.66%	70 s
WPFE feature	64.00%	37 s
Fusion feature	97.85%	43 s

As shown in **Table 2**, when WPE and WPFE were used as fused feature input to the GWO-LSTM, the classification accuracy significantly improved to 97.85%, surpassing the effect of WPE feature extraction and WPFE feature extraction. The runtime indicated that the model's convergence speed was faster. Meanwhile, after achieving high accuracy and low loss, the oscillation amplitude of training curve was noticeably lower compared to using WPE feature and WPFE feature. Because WPE feature can effectively distinguish the signals in the low and medium frequency ranges but lacks the ability to extract useful information in the high frequency range. WPFE feature can capture valuable information across the entire frequency range. Therefore, the fusion feature effectively compensates for deficiency of WPE feature in the high frequency range, resulting in higher accuracy and better efficiency.

Table 3. LSTM, GWO-SVM, GS-SVM, GWO-CNN model parameter settings.

Model	Parameter type	Value
LSTM	Number of cells per layer	20
	Learning rate	0.01
GWO-SVM	Optimization range of the C	$[2^{-3}, 2^{2}]$
	Optimization range of the γ	$[2^{-3}, 2^{2}]$
SVM	Optimization range of the C	$\{2^{-3}, 2^{-2}, \ldots, 2^{1}, 2^{2}\}$
	Optimization range of the γ	$\{2^{-3}, 2^{-2}, \ldots, 2^{1}, 2^{2}\}$
GWO-CNN	Optimization range of number of neuronal cells	[10,60]
	Optimization range of learning rate	[0.001,0.01]

Figure 13 shows the confusion matrix of classification results for the training and test sets when the WPE feature was imported in the GWO-LSTM. As shown in **Figure 13a**, the training set contains 2415 samples, including 541 samples with serious rattle noise, 924 samples with slight rattle noise, and 950 samples with no rattle noise. For label 1 (serious rattle noise), the recognition accuracy is 89.8%; for label 2 (slight rattle noise), the recognition accuracy is 93.5%; and for label 3 (no rattle noise), the recognition accuracy reaches 97.8%. As shown in **Figure 13b**, the test set consists of 1035 samples, including 235 samples with serious rattle noise, 401 samples with slight rattle noise, and 399 samples with no rattle noise. The recognition accuracy for label 1 in the test set is 88.5%, for label 2 is 90.0%, and for label 3 is 98.5%.

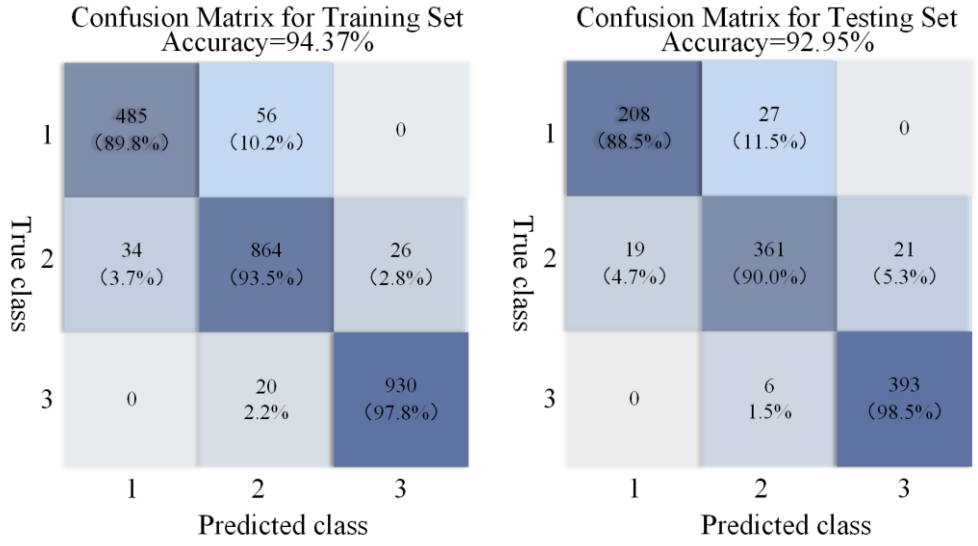

(a) **(b)**

Figure 13. Confusion matrix of WPE feature training set and testing set. **(a)** Training set; **(b)** Testing set.

Figure 14 illustrates the confusion matrix of the classification results for the training and test sets when the fusion feature was imported in the GWO-LSTM. In comparison, the classification performance of the fusion feature in both the training and test sets was superior to that of the single-feature input. By comparing **Figure 13a,b** with **Figure 14a,b**, it is clear that the recognition accuracy improved significantly across all three labels after feature fusion. This shows that the fusion feature can not only improve the model's recognition accuracy of shock absorber rattle noise, but also perform better in more complex classification status of no and slight rattle noise.

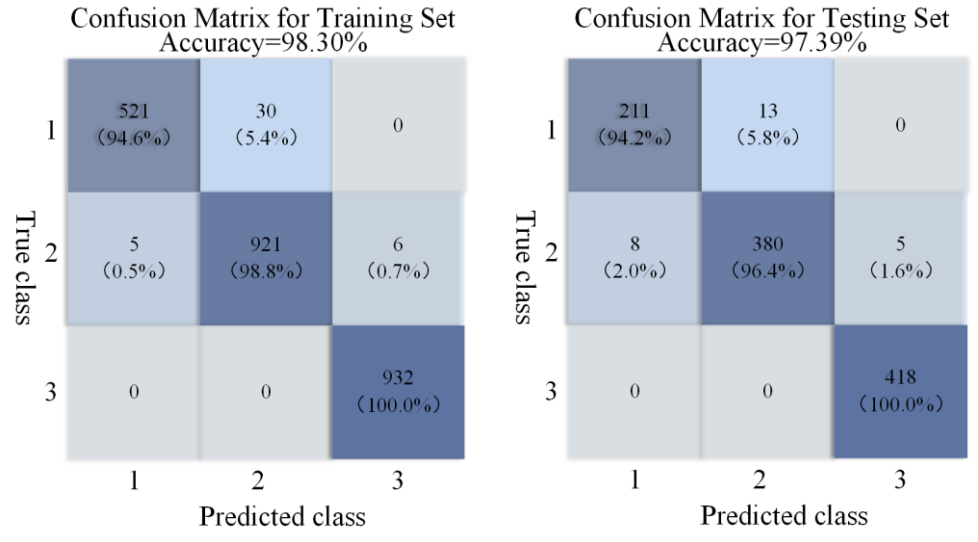

(a) **(b)**

Figure 14. Confusion matrix of fusion feature training set and testing set. **(a)** Training set; **(b)** Testing set.

4.3. Comparison with other models

The GWO-LSTM model to identify the fusion feature achieved significant result. The GWO-SVM model and GWO-CNN model have been achieved excellent effect in accuracy and efficiency in digital signal processing [44,45]. To further validate the classification accuracy and efficiency of the GWO-LSTM model, this study introduces four comparative models involving the traditional LSTM model, SVM model, GWO-SVM model and GWO-CNN model for identifying shock absorber rattle noise. In this process, the learning rate and the number of units in hidden layer for the LSTM model were set based on prior experience. The parameters C and γ for the GWO-SVM model were optimized using the GWO algorithm, while the parameters C and γ for the SVM model were optimized using a grid search method. The learning rate and the number of neuronal cells for the GWO-CNN model were optimized using the GWO algorithm. To ensure a fair comparison among these models, all of models utilized the same training and test sets as the GWO-LSTM model. **Table 3** presents the key parameter settings for the four models.

The predictive performance of the four models is shown in **Table 4**, and the classification results are further illustrated by the confusion matrix in **Figures 15** and **16**: **Figure 15a** for the LSTM model, **Figure 15b** for the GWO-SVM model, and **Figure 16a** for the SVM model, **Figure 16b** for the GWO-CNN model. As shown in **Figure 15a**, the traditional LSTM model achieved classification accuracies of 83.6%, 89.4%, and 94.8% for shock absorbers with serious rattle noise, slight rattle noise, and no rattle noise, respectively. The GWO-SVM model demonstrated even better classification performance across three levels rattle noise, particularly excelling in the classifications of no rattle noise and slight rattle noise, with accuracies of 97.5% and 98.4%, respectively. The GWO-CNN model was better than the GWO-SVM model in classifying the shock absorbers in the no rattle noise and serious rattle noise. Overall, the GWO-LSTM model surpassed the GWO-SVM, LSTM, SVM, and GWO-CNN models in classification accuracy, further confirming the effectiveness of the GWO-LSTM method in identifying rattle noise in shock absorbers. Additionally, the GWO-LSTM model outperformed the traditional LSTM, GWO-SVM and GWO-CNN models in terms of runtime, specifically taking 32 s for the traditional LSTM model, 121 s for the GWO-SVM model and 130 s for the GWO-CNN model. Based on the above analysis, it can be concluded that the GWO-LSTM model exhibits exceptional performance in identification of shock absorber rattle noise, both in classification accuracy and efficiency. Therefore, the GWO-LSTM model provides technical support for the automatic detection and classification of the rattle noise problem of the shock absorbers, and the accurate recognition effect is more convenient for the subsequent anti-noise design of the rattle noise shock absorber.

Table 4. Comparison of recognition effects.

Model	GWO-LSTM	LSTM	GWO-SVM	SVM	GWO-CNN
Recognition accuracy	97.85%	89.74%	96.02%	94.13%	96.97%
Recognition efficiency	43 s	32 s	121 s	50 s	130s

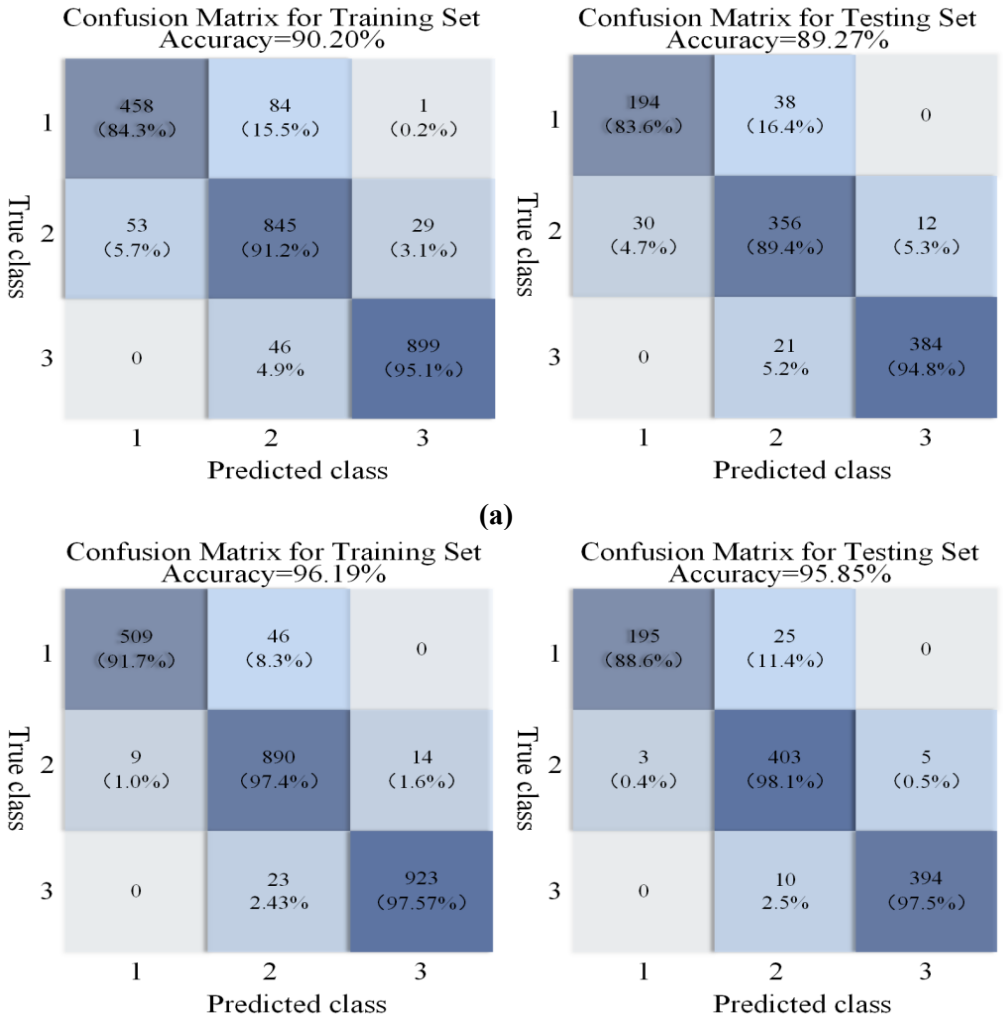

Figure 15. Confusion matrix of training and testing sets of different models. **(a)** LSTM training and testing set; **(b)** GWO-SVM training and testing set.

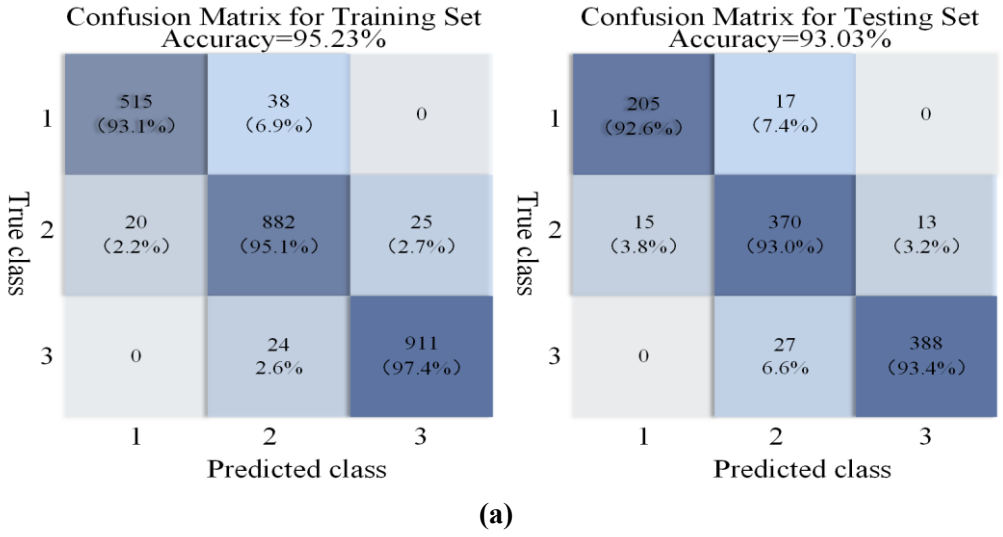

(b)

Figure 16. Confusion matrix of training and testing sets of different models. **(a)** SVM training and testing set; **(b)** GWO-CNN training and testing set.

To further validate the high accuracy of the models, two statistics, mean and standard deviation, were introduced to measure the stability of the results of 20 computational experiments for the five model. As shown in **Table 5**, the mean and standard deviation of the recognition accuracy of the five models were compared, respectively. The standard deviation of each model was less than 0.1, indicating that the fluctuation of the results of each model was very small and had a strong credibility.

Table 5. Comparison of the mean and standard deviation.

Model	GWO-LSTM	LSTM	GWO-SVM	SVM	GWO-CNN
Mean	97.85%	89.74%	96.02%	94.13%	96.97%
Standard Deviation	0.053	0.046	0.009	0.005	0.004

5. Conclusions

This paper presents a method for recognizing shock absorber rattle noise based on wavelet packet feature fusion and the GWO-LSTM model. By integrating WPE and WPFE features, and optimizing the hyperparameters of the LSTM model using the GWO, accurate identification of different rattle noise levels is achieved. Considering the cost of experimentation, a total of 50 shock absorbers were tested both in road and rig test, generating 3450 valid experimental samples. Experimental results indicate that the fused feature significantly improves classification accuracy, with the GWO-LSTM model achieving an accuracy rate of 97.85%, especially in distinguishing between no rattle noise and slight rattle noise. This performance surpasses that of traditional models such as LSTM, SVM, and GWO-SVM. Moreover, the GWO-LSTM model exhibits superior training efficiency. The findings demonstrate that the combination of wavelet packet feature fusion with GWO optimization enhances the accuracy and robustness of shock absorber noise recognition.

The proposed method can be retrained and extended to solve other fault identification problems. In addition, the method can provide valuable technical

support for the automated detection and classification of the shock absorber rattle noise problem. For example, the system of shock absorber rattle noise analysis and detection can be designed and developed to provide guidance for anti-rattle noise design of shock absorber.

Author contributions: Conceptualization, JH and XH; methodology, JH; software, JH; validation, HY, XX and XN; formal analysis, RD; investigation, JH; resources, XH; data curation, JH, HY and XX; writing—original draft preparation, JH; writing—review and editing, JH and XH; visualization, JH and RD; supervision, XH; project administration, XH; funding acquisition, XN. All authors have read and agreed to the published version of the manuscript.

Funding: Fund for Sichuan Science and Technology Program (2023YFH0065), and Basic Research of Jiangsu Provincial Department of Science and Technology (Natural Science Foundation, No. BK20231178).

Acknowledgments: The authors would like to acknowledge the support from the Institute of Energy and Power Research for the experimental research.

Availability of data and materials: The authors do not have permission to share the data.

Conflict of interest: The authors declare no conflict of interest.

References

1. Zhu H, Zhao J, Wang Y, et al. Improving of pure electric vehicle sound and vibration comfort using a multi-task learning with task-dependent weighting method. Measurement. 2024; 233: 114752. doi: 10.1016/j.measurement.2024.114752
2. Hua X, Thomas A, Shultis K. Recent progress in battery electric vehicle noise, vibration, and harshness. Science Progress. 2021; 104(1).
3. Fan D, Dai P, Yang M, et al. Research on Maglev Vibration Isolation Technology for Vehicle Road Noise Control. SAE International Journal of Vehicle Dynamics, Stability, and NVH. 2022; 6(3): 233–245. doi: 10.4271/10-06-03-0016
4. Huang HB, Li RX, Huang XR, et al. Identification of vehicle suspension shock absorber squeak and rattle noise based on wavelet packet transforms and a genetic algorithm-support vector machine. Applied Acoustics. 2016; 113: 137–148. doi: 10.1016/j.apacoust.2016.06.016
5. Benaziz M, Nacivet S, Deak J, Thouverez F. Double Tube Shock Absorber Model for Noise and Vibration Analysis. SAE International Journal of Passenger Cars-Mechanical Systems. 2013; 6(2): 1177–1185. doi: 10.4271/2013-01-1912
6. Huang HB, Li RX, Yang ML, et al. Evaluation of vehicle interior sound quality using a continuous restricted Boltzmann machine-based DBN. Mechanical Systems and Signal Processing. 2017; 84: 245–267. doi: 10.1016/j.ymssp.2016.07.014
7. Huang Y, Li D. Subjective discomfort model of the micro commercial vehicle vibration over different road conditions. Applied Acoustics. 2019; 145: 385–392. doi: 10.1016/j.apacoust.2018.10.028
8. Benaziz M, Nacivet S, Thouverez F. A shock absorber model for structure-borne noise analyses. Journal of Sound and Vibration. 2015; 349: 177–194. doi: 10.1016/j.jsv.2015.03.034
9. Zheng T, Zheng Y, Gong X, et al. Diagnosis and analysis of twin-tube shock absorber rattling noise in electric vehicle. Vibroengineering Procedia. 2022; 42: 57–63. doi: 10.21595/vp.2022.22606
10. Bogema D, Goodes P, Apelian C, Csakan M. Noise path analysis process evaluation of automotive shock absorber transient noise. Available online: https://doi.org/10.4271/2009-01-2091 (accessed on 20 October 2024)
11. Huang HB, Huang XR, Wu JH, et al. Novel method for identifying and diagnosing electric vehicle shock absorber squeak noise based on a DNN. Mechanical Systems and Signal Processing. 2019; 124: 439–458. doi: 10.1016/j.ymssp.2019.01.053
12. Michalakoudis I, Thite AN. Experimental identification of shock absorber knocking noise using various input waveforms. Noise Control Engineering Journal. 2013; 61(1): 26–40. doi: 10.3397/1/1.3761003

13. Sacramento G, Biera J. Simulation tool for shock absorber noise prediction in time and frequency domains. International Journal of Vehicle Noise and Vibration. 2007; 3(3): 217–229. doi: 10.1504/ijvnv.2007.015174
14. Huang H, Huang X, Ding W, et al. Uncertainty optimization of pure electric vehicle interior tire/road noise comfort based on data-driven. Mechanical Systems and Signal Processing. 2022; 165: 108300. doi: 10.1016/j.ymssp.2021.108300
15. Huang H, Huang X, Ding W, et al. Optimization of electric vehicle sound package based on LSTM with an adaptive learning rate forest and multiple-level multiple-object method. Mechanical Systems and Signal Processing. 2023; 187: 109932. doi: 10.1016/j.ymssp.2022.109932
16. Wang H, Wu X, Huang Z, Xing EP. (2020). High-frequency component helps explain the generalization of convolutional neural networks. In: Proceedings of the IEEE/CVF conference on computer vision and pattern recognition; 13–19 June 2020; Seattle, WA, USA. pp. 8684–8694.
17. Hatta NM, Zain AM, Sallehuddin R, et al. Recent studies on optimisation method of Grey Wolf Optimiser (GWO): a review (2014–2017). Artificial Intelligence Review. 2018; 52(4): 2651–2683. doi: 10.1007/s10462-018-9634-2.
18. Mirjalili S, Mirjalili SM, Lewis A. Grey Wolf Optimizer. Advances in Engineering Software. 2014; 69: 46–61. doi: 10.1016/j.advengsoft.2013.12.007
19. Zhao W, Yang Y, Lu Z. Interval Short-Term Traffic Flow Prediction Method Based on CEEMDAN-SE Nosie Reduction and LSTM Optimized by GWO. Wireless Communications and Mobile Computing. 2022; 2022(1): 5257353.
20. Huang HB, Li RX, Ding WP, et al. Rig test for identifying abnormal noise of suspension shock absorber (Chinese). Journal of Vibration and Shock. 2015; 34(2): 191–196. doi: 10.13465/j.cnki.jvs.2015.02.034
21. Huang HB, Li RX, Huang XR, et al. Sound quality evaluation of vehicle suspension shock absorber rattling noise based on the Wigner–Ville distribution. Applied Acoustics. 2015; 100: 18–25. doi: 10.1016/j.apacoust.2015.06.018
22. orres R, Torres E. Fractional Fourier Analysis of Random Signals and the Notion of /spl alpha/-Stationarity of the Wigner–Ville Distribution. IEEE Transactions on Signal Processing. 2013; 61(6): 1555–1560. doi: 10.1109/TSP.2012.2236834
23. McLoughlin I, Xie Z, Song Y, et al. Time–Frequency Feature Fusion for Noise Robust Audio Event Classification. Circuits, Systems, and Signal Processing. 2020; 39(3): 1672–1687. doi: 10.1007/s00034-019-01203-0
24. Jayasree T, Ananth RP. Sound Signal Based Fault Classification System in Motorcycles Using Hybrid Feature Sets and Extreme Learning Machine Classifiers. Sound and Vibration. 2020; 54(1): 57–74. doi: 10.32604/sv.2020.08573
25. Zhao J, Yin YQ, Chen JF, et al. Evaluation and Prediction of Vibration Comfort in Engineering Machinery Cabs Using Random Forest with Genetic Algorithm. SAE International Journal of Vehicle Dynamics, Stability, and NVH. 2024; 8(4): 491–512. doi: 10.4271/10-08-04-0027
26. Jing YB, Liu CW, Bi FR, et al. Diesel engine valve clearance fault diagnosis based on features extraction techniques and FastICA-SVM. Chinese Journal of Mechanical Engineering. 2017; 30: 991–1007. doi: 10.1007/s10033-017-0140-2
27. Cody MA. The wavelet packet transform: Extending the wavelet transform. Dr. Dobb's Journal. 1994; 19: 44–46.
28. Sarikaya R, Pellom BL, Hansen JH. Wavelet packet transform features with application to speaker identification. In: Proceedings of the IEEE Nordic Signal Processing Symposium; 8–11 June 1998; Vigsø, Denmark. pp. 81–84.
29. Chen G, Li QY, Li DQ, et al. Main frequency band of blast vibration signal based on wavelet packet transform. Applied Mathematical Modelling. 2019; 74: 569–585. doi: 10.1016/j.apm.2019.05.005
30. Algumaei M, Hettiarachchi IT, Veerabhadrappa R, Bhatti A. Wavelet packet energy features for eeg-based emotion recognition. In: Proceedings of the 2021 IEEE International Conference on Systems, Man, and Cybernetics (SMC); 17–20 October 2021; Melbourne, Australia. pp. 1935–1940.
31. Huang H, Wang Y, Wu J, et al. Prediction and optimization of pure electric vehicle tire/road structure-borne noise based on knowledge graph and multi-task ResNet. Expert Systems with Applications. 2024; 255: 124536. doi: 10.1016/j.eswa.2024.124536
32. Nason GP, Sapatinas T. Wavelet packet transfer function modelling of nonstationary time series. Statistics and Computing. 2002; 12: 45–56. doi: 10.1023/A:1013168221710
33. Varanis M, Pederiva R. Statements on wavelet packet energy–entropy signatures and filter influence in fault diagnosis of induction motor in non-stationary operations. Journal of the Brazilian Society of Mechanical Sciences and Engineering. 2018; 40(2). doi: 10.1007/s40430-018-1025-8
34. Wang S, Yang X, Zhang Y, et al. Identification of Green, Oolong and Black Teas in China via Wavelet Packet Entropy and Fuzzy Support Vector Machine. Entropy. 2015; 17(10): 6663–6682. doi: 10.3390/e17106663

35. Pang J, Mao T, Jia W, et al. Prediction and Analysis of Vehicle Interior Road Noise Based on Mechanism and Data Series Modeling. Sound & Vibration. 2024; 58(1): 59–80. doi: 10.32604/sv.2024.046247
36. Zhao Z, Chen W, Wu X, et al. LSTM network: a deep learning approach for short-term traffic forecast. IET Intelligent Transport Systems. 2017; 11(2): 68–75. doi: 10.1049/iet-its.2016.0208
37. Yu Y, Si X, Hu C, Zhang J. A review of recurrent neural networks: LSTM cells and network architectures. Neural computation. 2019; 31(7): 1235–1270. https://doi.org/10.1162/neco_a_01199
38. Tian Y, Yu J, Zhao A. Predictive model of energy consumption for office building by using improved GWO-BP. Energy Reports. 2020; 6: 620–627. doi: 10.1016/j.egyr.2020.03.003
39. Yildirim Ö. A novel wavelet sequence based on deep bidirectional LSTM network model for ECG signal classification. Computers in Biology and Medicine. 2018; 96: 189–202. doi: 10.1016/j.compbiomed.2018.03.016
40. Shoeibi M, Nevisi MMS, Salehi R, et al. Enhancing Hyper-Spectral Image Classification with Reinforcement Learning and Advanced Multi-Objective Binary Grey Wolf Optimization. Computers, Materials & Continua. 2024; 79(3): 3469–3493. doi: 10.32604/cmc.2024.049847
41. Liao X, Zhou G, Zhang Z, et al. Tool wear state recognition based on GWO–SVM with feature selection of genetic algorithm. The International Journal of Advanced Manufacturing Technology. 2019; 104(1–4): 1051–1063. doi: 10.1007/s00170-019-03906-9
42. Pan J, Jing B, Jiao X, Wang S. Analysis and Application of Grey Wolf Optimizer-Long Short-Term Memory. IEEE Access. 2020; 8: 121460–121468. doi: 10.1109/access.2020.3006499
43. Huang HB, Huang XR, Li RX, et al. Sound quality prediction of vehicle interior noise using deep belief networks. Applied Acoustics. 2016; 113: 149–161. doi: 10.1016/j.apacoust.2016.06.021
44. Ma J, Fan L, Tian W, Miao ZH. Research on Data Classification Method of Optimized Support Vector Machine Based on Gray Wolf Algorithm. International Journal of Grid and High Performance Computing. 2023; 15(2): 1–14. doi: 10.4018/ijghpc.318408
45. Bilal A, Sun G, Mazhar S, Imran A. (2022). Improved grey wolf optimization-based feature selection and classification using CNN for diabetic retinopathy detection. In: Proceedings of the ICECMSN 2021: 2nd International Conference on Evolutionary Computing and Mobile Sustainable Networks; 20–21 May 2021; Bangalore, India. pp. 1–14.